HEALTH AND MEDICINE

Engineered botulinum neurotoxin B with improved binding to human receptors has enhanced efficacy in preclinical models

Mark Elliott[1]*, Christine Favre-Guilmard[2]*, Sai Man Liu[1]*, Jacquie Maignel[2]*, Geoffrey Masuyer[3]*, Matthew Beard[1†], Christopher Boone[4†], Denis Carré[2†], Mikhail Kalinichev[2†], Stephane Lezmi[2†], Imran Mir[1†], Camille Nicoleau[2†], Shilpa Palan[1†], Cindy Perier[2†], Elsa Raban[2†], Sicai Zhang[4†], Min Dong[4‡], Pål Stenmark[3,5‡], Johannes Krupp[1,2‡]

Although botulinum neurotoxin serotype A (BoNT/A) products are common treatments for various disorders, there is only one commercial BoNT/B product, whose low potency, likely stemming from low affinity toward its human receptor synaptotagmin 2 (hSyt2), has limited its therapeutic usefulness. We express and characterize two full-length recombinant BoNT/B1 proteins containing designed mutations E1191M/S1199Y (rBoNT/B1$_{MY}$) and E1191Q/S1199W (rBoNT/B1$_{QW}$) that enhance binding to hSyt2. In preclinical models including human-induced pluripotent stem cell neurons and a humanized transgenic mouse, this increased hSyt2 affinity results in high potency, comparable to that of BoNT/A. Last, we solve the cocrystal structure of rBoNT/B1$_{MY}$ in complex with peptides of hSyt2 and its homolog hSyt1. We demonstrate that neuronal surface receptor binding limits the clinical efficacy of unmodified BoNT/B and that modified BoNT/B proteins have promising clinical potential.

INTRODUCTION

Botulinum neurotoxins are a family of potent bacterial toxins, including seven major serotypes (BoNT/A to BoNT/G) and many subtypes (designated with numerical number, e.g., BoNT/A1). Because of their highly specific action on blocking neurotransmission, BoNTs are used for the treatment of muscle hypertonicity in various medical indications (*1*, *2*). Treatment consists of injecting the BoNT-containing product directly into affected areas and is typically well tolerated (*2*, *3*). However, generation of neutralizing antibodies that renders future treatments ineffective can occur (*4*). Adverse effects that are sometimes associated with BoNT treatment seem linked to unwanted spread and diffusion of the toxin away from the site of injection (*5*, *6*). In the clinical setting, multiple factors influence this unwanted spread and diffusion, with the administered dose being a recognized factor affecting toxin spread (*7*).

Most available BoNT therapeutics are derived from BoNT/A1, with just one commercial BoNT/B1 product (*2*). In clinical practice, the latter displays a lower potency than the available BoNT/A1 products, commonly necessitating the administration of higher doses of the BoNT/B1 product (*8*) and leading to a higher frequency of clinically undesirable effects (*2*, *9*). A BoNT/B1 protein engineered to require doses as low as the available BoNT/A1 products thus has the potential to match the efficacy and safety profile of the BoNT/A1 products.

The prospect of developing an engineered BoNT/B1 protein with these properties has come into view after recent insights into the way that BoNT/B1 interacts with the membrane proteins of the targeted neuron. Unlike BoNT/A, which uses synaptic vesicle protein 2 isoforms A to C, BoNT/B recognizes synaptotagmins 1 and 2 (Syt1 and Syt2, respectively) (*10*, *11*). Of these two isoforms, Syt2 appears to be the major isoform at the mature neuromuscular junction (NMJ) (*12*). BoNT/B1 displays a higher affinity to the rodent homolog of Syt2 as compared to the human homolog (*13*, *14*). The molecular basis of this interaction has been determined by x-ray crystallography (*15*). Using a bacterial adenylate cyclase two-hybrid saturation mutagenesis screen, we previously identified a series of point mutations that can be introduced into the receptor-binding domain of BoNT/B (Hc/B) to enhance its binding to human receptor Syt2 (hSyt2) (*16*). Furthermore, introducing an E1191M/S1199Y double mutation to the full-length molecule [recombinant BoNT (rBoNT)/B1$_{MY}$] was shown to have increased functional efficacy in cultured rodent neurons that expressed hSyt2 via lentiviral transduction (*16*). Notably, the toxin used in this earlier study was a histidine-tagged version.

Here, we produce the full-length rBoNT/B1$_{MY}$ without this histidine tag, as well as a second untagged modified toxin containing a different set of mutations (E1191Q/S1199W; rBoNT/B1$_{QW}$). We characterize the activity of both toxins in several preclinical models including human neurons derived from induced pluripotent stem cells (iPSCs) and a humanized transgenic mouse model that expresses the hSyt2 toxin binding region. Our studies demonstrate that the increased affinity to the human receptor results in increased activity of both modified toxins in these models with a potency similar to that of rBoNT/A1. Our data demonstrate that neuronal surface receptor binding is likely to be the major factor limiting the clinical efficacy of BoNT/B1. Furthermore, we also solve the crystal structures of rBoNT/B1$_{MY}$ in complex with both human Syt isoforms, as well as a molecular basis for their interactions.

[1]Ipsen Bioinnovation, 102 Park Drive, Milton Park, Abingdon OX14 4RY, UK. [2]Ipsen Innovation, 5 Avenue du Canada, 91940 Les Ulis, France. [3]Department of Biochemistry and Biophysics, Stockholm University, Stockholm SE-106 91, Sweden. [4]Department of Urology, Boston Children's Hospital, Department of Microbiology and Immunobiology and Department of Surgery, Harvard Medical School, Boston, MA 02115, USA. [5]Department of Experimental Medical Science, Lund University, 221 00 Lund, Sweden.
*These authors contributed equally to this work as first authors.
†These authors contributed equally to this work as second authors.
‡Corresponding author. Email: johannes.krupp@ipsen.com (J.K.); min.dong@childrens.harvard.edu (M.D.); stenmark@dbb.su.se (P.S.)

In addition, we report the cocrystal structure of BoNT/B1 in complex with Syt1. Our data suggest that rBoNT/$B1_{MY}$ and rBoNT/$B1_{QW}$ are interesting candidates to be developed into new clinical treatment options for patients suffering from a spectrum of disorders.

RESULTS

rBoNT/$B1_{MY}$ and rBoNT/$B1_{QW}$ have higher activity than rBoNT/B1 in cell-based assays

To characterize the biological activity of the enzymatically active toxins, we first tested the efficacy of blocking [^{3}H]-glycine release from primary rat spinal cord neurons (SCNs). The toxin concentration required for 50% maximal inhibition (IC_{50}) of [^{3}H]-glycine release was 1.1 pM for rBoNT/$B1_{MY}$ and rBoNT/$B1_{QW}$ ($n = 3$ for both toxins), demonstrating functionality of both modified toxins (Fig. 1A). For comparison, the IC_{50} for rBoNT/B1 in this assay was 3.5 pM ($n = 4$).

We next characterized the activity of rBoNT/$B1_{MY}$ and rBoNT/$B1_{QW}$ in various human-derived or humanized models, henceforth including rBoNT/A1 and rBoNT/B1 for comparison. We first tested the toxins on neurons derived from human iPSCs (hiPSCs), iCell GABANeurons, which have been shown to be highly sensitive to BoNTs (*17*). As hypothesized from the increased affinity of both mutants to hSyt1 and hSyt2 (table S1), the IC_{50} of [^{3}H]–γ-aminobutyric acid (GABA) release was significantly lower for the two rBoNT/B1 mutants as compared to unmodified rBoNT/B1 [0.3 pM for rBoNT/$B1_{MY}$ and rBoNT/$B1_{QW}$ ($n = 3$ for each toxin) versus 10.7 pM for rBoNT/B1 ($n = 4$); Fig. 1B]. Likewise, the IC_{50} for the two rBoNT/B1 mutants was also significantly lower as compared to rBoNT/A1, which had an IC_{50} of 2.3 pM ($n = 5$). Analysis of the expression levels of Syt1 and Syt2 confirmed the presence of both isoforms at the time when GABA release assays were performed (16 to 18 days in vitro; fig. S1A). The presence of other proteins involved in soluble NSF (*N*-ethylmaleimide–sensitive factor) attachment protein receptor (SNARE)–mediated release in these cells was also confirmed (fig. S1B). Note that the values reported in table S1 reflect on the binding of the BoNT/B mutants to the Syt isoforms only, without the ganglioside co-receptor. In the functional studies, the BoNT/B toxins will have a much higher affinity to the neuronal surfaces since they can interact with the Syt isoforms and the ganglioside co-receptor.

A transgenic mouse model with a humanized luminal domain of Syt2

To further assess the activity of modified rBoNT/$B1_{MY}$ and rBoNT/$B1_{QW}$ in models that express the hSyt2 toxin binding site (Fig. 2A), we generated transgenic mice in which the luminal domain of the murine Syt2 was replaced by the human sequence (hereafter referred to as "hSyt2 mice"). These transgenic mice were viable, but their fertility rate was reduced. Husbandry data were consistent with the idea that this was due to partial male infertility (Fig. 2B). Phenotypic characterization of the mice did not indicate other abnormalities; for example, hSyt2 mice displayed normal body weights (BWs) (Fig. 2C) with no signs of ataxia when compared to wild-type (WT) mice. Likewise, histopathological analysis of several tissues did not detect any differences between the hSyt2 mice and their WT littermates. Distribution of Syt1, Syt2, and other proteins involved with central nervous system synaptic function was not different between hSyt2 and WT mice (Fig. 2, D and E).

Syt2 has a major role in mediating toxin efficacy in the hemidiaphragm muscle but not in the detrusor smooth muscle

The activity of the toxins (10 pM) was assessed in phrenic nerve hemidiaphragm striated muscle prepared from hSyt2 mice and compared to those from WT littermates. In hSyt2 tissue, the time taken to achieve half-maximal paralysis (t_{50}) for electrically evoked hemidiaphragm muscle contractions was 53.7 ± 3.3 min ($n = 5$) and 121.2 ± 4.8 min ($n = 6$) for rBoNT/A1 and rBoNT/B1, respectively. This compared to 53.9 ± 3.5 min ($n = 5$) and 60.3 ± 6.3 min ($n = 4$)

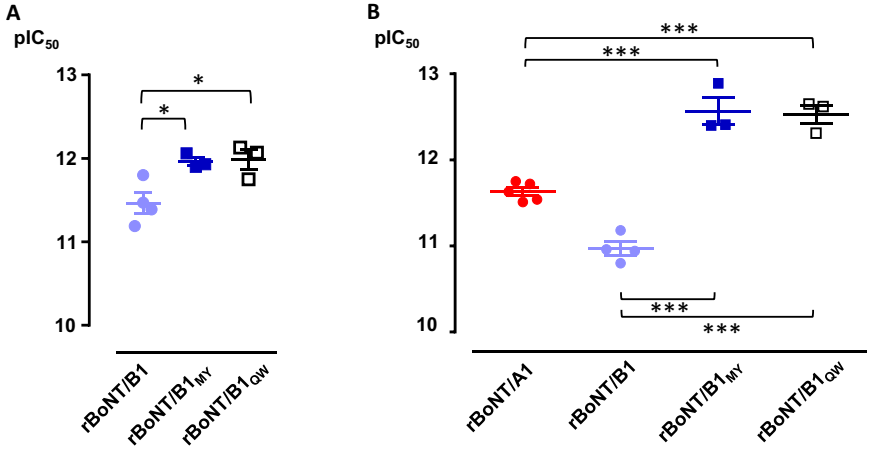

Fig. 1. Engineered rBoNT/B1 toxins inhibit neurotransmitter release with higher potency than rBoNT/B1. (**A**) Inhibition of [^{3}H]-glycine release from primary rat SCNs by rBoNT/B1, rBoNT/$B1_{MY}$, or rBoNT/$B1_{QW}$. The logarithmic concentration of each toxin required for IC_{50} (pIC_{50}) of [^{3}H]-glycine release was 11.46 ± 0.13 ($n = 4$), 11.96 ± 0.05 ($n = 3$), and 11.98 ± 0.12 ($n = 3$) for rBoNT/B1, rBoNT/$B1_{MY}$, and rBoNT/$B1_{QW}$, respectively. *$P < 0.05$, Tukey's multiple comparison. Maximum achieved mean inhibition of the release was 82.4, 85.1, and 85.2% for rBoNT/B1, rBoNT/$B1_{MY}$, and rBoNT/$B1_{QW}$, respectively. (**B**) Inhibition of [^{3}H]-GABA release from human iCell GABANeurons by rBoNT/A1, rBoNT/B1, rBoNT/$B1_{MY}$, or rBoNT/$B1_{QW}$. The pIC_{50} of [^{3}H]-GABA release was 11.63 ± 0.05 ($n = 5$), 10.97 ± 0.08 ($n = 4$), 12.57 ± 0.16 ($n = 3$), and 12.53 ± 0.11 ($n = 3$) for rBoNT/A1, rBoNT/B1, rBoNT/$B1_{MY}$, and rBoNT/$B1_{QW}$, respectively. ***$P < 0.0001$, analysis of variance (ANOVA) followed by Tukey's multiple comparison. Maximum achieved mean inhibition of the release was 91.4, 94.1, 89.5, and 70.8% for rBoNT/B1, rBoNT/$B1_{MY}$, rBoNT/$B1_{QW}$, and rBoNT/A1, respectively.

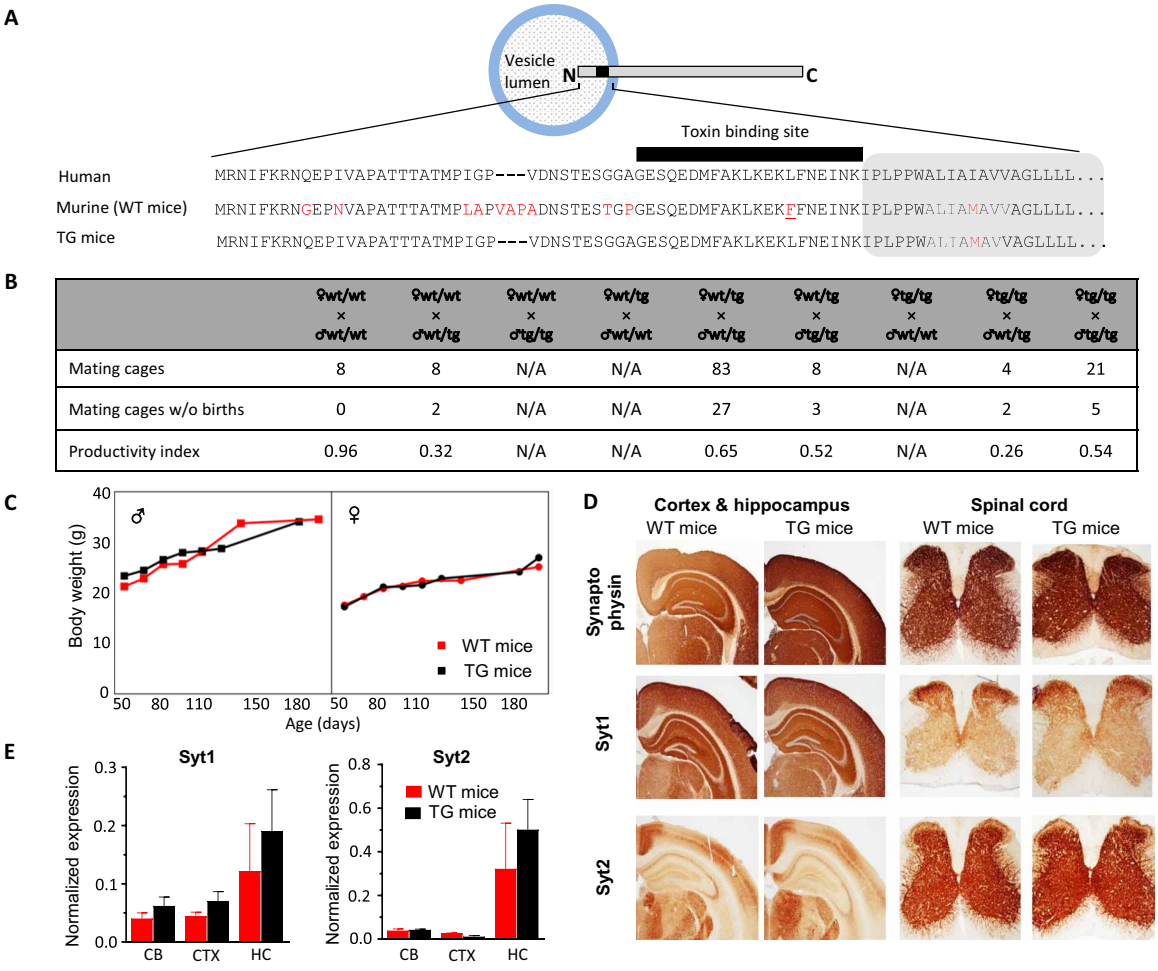

	♀wt/wt × ♂wt/wt	♀wt/wt × ♂wt/tg	♀wt/wt × ♂tg/tg	♀wt/tg × ♂wt/wt	♀wt/tg × ♂wt/tg	♀wt/tg × ♂tg/tg	♀tg/tg × ♂wt/wt	♀tg/tg × ♂wt/tg	♀tg/tg × ♂tg/tg
Mating cages	8	8	N/A	N/A	83	8	N/A	4	21
Mating cages w/o births	0	2	N/A	N/A	27	3	N/A	2	5
Productivity index	0.96	0.32	N/A	N/A	0.65	0.52	N/A	0.26	0.54

Fig. 2. Characterization of a transgenic mouse strain in which the luminal domain of Syt2 is replaced by the human sequence. (**A**) Schematic representation of Syt2 (left) and sequence alignment of the human and murine vesicle luminal domains (right). Non-identical residues are highlighted in red, including F at position 54 of the murine sequence (red underlined). Transgenic mice (TG) incorporate the entire human luminal domain, as shown. (**B**) Breeding data of WT and various genotypes of transgenic mice. All tested breeding groups produced offspring; however, the productivity index (defined as number of pups per female per week) for groups where the male animals had at least one transgenic allele (tg) was lower than WT mice, which always produced offspring. These results are consistent with a dominant partial male infertility of the modified Syt2. N/A, not assessed. (**C**) Transgenic mice homozygotes show a normal BW to age profile compared to WT homozygotes (3 to 41 animals per data point). (**D**) Immunohistochemistry data showing that the expression pattern of Syt1 and Syt2 in brain and spinal cord of transgenic animals was not different as compared to homozygotic WT animals. (**E**) The expression levels of Syt1 and Syt2 in the cerebellum (CB), cortex (CTX), and hippocampus (HC) of homozygotic transgenic animals was assessed by Western blot analysis. Values are normalized to expression of SNAP-25 in each preparation. There was no significant difference for any of the brain regions or Syt isoforms between transgenic mice and WT animals ($P > 0.05$, paired t test).

in WT tissue, respectively. The difference between hSyt2 and WT mice values was significant for rBoNT/B1 ($P < 0.0001$, unpaired t test; Fig. 3, A and D), suggesting that the activity of BoNT/B1 in the hemidiaphragm model is, to a large degree, mediated through interaction with Syt2. The t_{50} in hSyt2 tissue for rBoNT/B1$_{MY}$ (Fig. 3B) and rBoNT/B1$_{QW}$ (Fig. 3C) was 62.5 ± 4.7 min (n = 7) and 71.8 ± 3.0 min (n = 6), respectively. These values were not significantly different to those obtained in tissue from WT littermates with these two toxins [t_{50} = 54.3 ± 3.9 min (n = 5) and 69.2 ± 3.5 min (n = 5), respectively; Fig. 3D), consistent with the idea that the mutations, while improving affinity to hSyt2, only have minor effects on the affinity to murine Syt2, as compared to rBoNT/B1 (table S1). The potency of the mutated toxins was significantly higher in hSyt2 mice as compared to rBoNT/B1 [$P < 0.0001$, one-way analysis of variance (ANOVA) followed by Tukey's multiple comparison], but there was no significant difference between mutated and WT rBoNT/B1 toxins in WT mice (Fig. 3D).

We next tested the toxins in a mouse detrusor smooth muscle preparation. As reported earlier (*18*), low nanomolar concentrations of toxins are needed to induce paralysis in this tissue. In our studies, contraction strength was gradually reduced in both the WT and the hSyt2 mice after bath application of 1 nM toxins (Fig. 4, A and B). In contrast to the hemidiaphragm striated muscle, rBoNT/B1 had similar activity in detrusor smooth muscle tissue from WT and hSyt2 mice with 55.2 ± 3.8 min (n = 5) and 57.3 ± 3.6 min (n = 5), respectively. Likewise, both mutants had similar high activity in WT and hSyt2 preparations. The t_{50} values were 38.7 ± 4.4 min (n = 5) and 39.4 ± 3.8 min (n = 3) in WT tissue and 40.2 ± 3.2 min (n = 4) and 37.1 ± 0.9 min (n = 3) in hSyt2 tissue for rBoNT/B1$_{MY}$ and rBoNT/B1$_{QW}$, respectively (Fig. 4C). Although the values for the

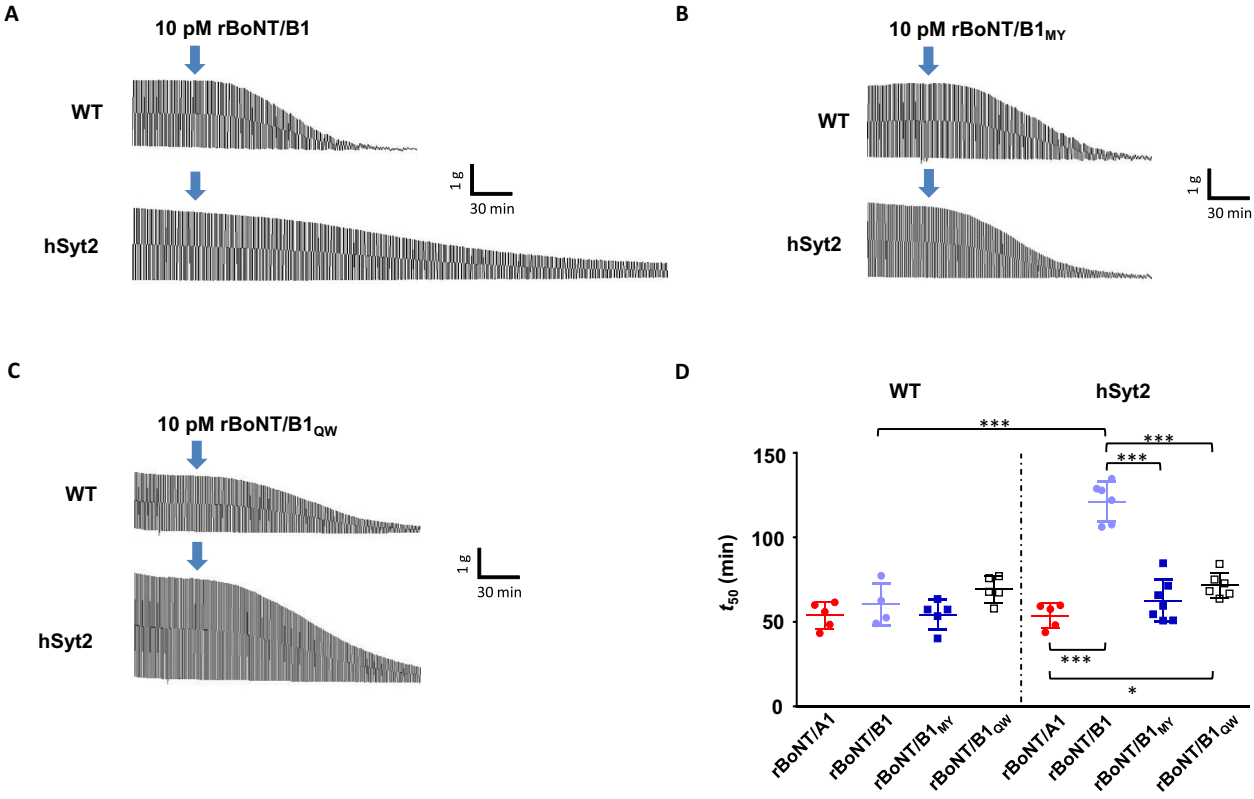

Fig. 3. Engineered rBoNT/B1, but not rBoNT/B1, toxins induce rapid hemidiaphragm paralysis in hSyt2 mice. (**A** to **C**) Contractile force of the hemidiaphragm muscle plotted over time from WT or hSyt2 mice. The phrenic nerve was stimulated at a frequency of 1 Hz with a 20-μs pulse duration. Following tissue stabilization, a toxin was added (blue arrows) to the bath at a final concentration of 10 pM. Whereas rBoNT/B1 induced a rapid paralysis of the muscle from WT mice, paralysis was significantly attenuated ($P < 0.0001$, unpaired t test) in tissue prepared from hSyt2 mice (A). In contrast, both rBoNT/$B1_{MY}$ (B) and rBoNT/$B1_{QW}$ (C) induced a rapid paralysis in hemidiaphragm preparations from both WT and hSyt2 mice. (**D**) All data were normalized to the contractile strength before toxin addition and fitted to a four-parameter equation to determine t_{50}. Unpaired t test was used to compare datasets between WT and hSyt2 mice for each toxin. Datasets for all toxins per WT or hSyt2 mice were compared with ANOVA followed by Tukey's test for multiple comparisons. *$P < 0.05$, ***$P < 0.0001$. All other comparisons were not significant.

mutants were, in WT and hSyt2 tissue, lower than those for the unmodified rBoNT/B1, this was not statistically significant. These data suggest that Syt1, rather than Syt2, plays a major role in mediating toxin efficacy in bladder smooth muscle. This was corroborated by immunohistochemical (IHC) analysis, which consistently detected immunoreactivity for Syt1 in the bladder tissue from WT and hSyt2 mice but failed to detect staining for Syt2 in either preparation, despite positive signals in spinal cord control preparations (Fig. 4D). As expected from previous work with natural toxins (*19*), rBoNT/A1 had significantly lower rates of blockade than the rBoNT/B1 toxins in the smooth muscle bladder preparation (hSyt2 mice, t_{50} = 106.6 ± 7.3 min (n = 4); WT mice, t_{50} = 112.4 ± 8.2 min (n = 5); Fig. 4C).

The in vivo activity of rBoNT/$B1_{MY}$ and rBoNT/$B1_{QW}$ matches that of rBoNT/A1

We next used the digit abduction scoring (DAS) assay in mice (*20*) to test the activity of the toxins in vivo. In WT mice, rBoNT/A1 and rBoNT/B1 had similar high activity with half-maximal effective dose (ED_{50}) values close to 1 pg per animal (table S2). As expected, rBoNT/A1 potency was unchanged in the hSyt2 mice, but rBoNT/B1 had reduced DAS scores, and the ED_{50} value was approximately fourfold higher than that in WT animals (Fig. 5A and table S2). In contrast, rBoNT/$B1_{MY}$ and rBoNT/$B1_{QW}$ induced muscle weakness in the hSyt2 mice with ED_{50} values close to 1 pg per animal. ED_{50} values with the modified toxins in the WT mice were close to 1.5 pg per animal (Fig. 5A and Table S2).

Transient BoNT dose-dependent BW loss is considered evidence of a generalized toxin effect in mice (*21*). Thus, BW was assessed in parallel to the daily DAS measurement. The 0% BW dose was higher than the respective ED_{50} values for all toxins in WT and hSyt2 mice (table S2). The tolerability index of the toxins, defined as the ratio between the calculated dose inducing Δ 0% BW and DAS ED_{50}, was similar for all toxins in both WT and transgenic mice (Table S2).

Besides humans, five other species were found to present a leucine at position 54 (murine sequence numbering) in Syt2, including gorilla, chimpanzee, mole rat, kangaroo rat, and lesser hedgehog (fig. S2A). Using a Syt2 peptide representing the sequence of the kangaroo rat, we confirmed that the presence of the leucine residue at this position reduced the interaction with BoNT/B (fig. S2, B and C).

Considering that results in the WT mice for rBoNT/$B1_{MY}$ and rBoNT/$B1_{QW}$ did not overestimate the activity of the toxins in the hSyt2 mice (table S2), we next tested one of the two modified toxins, rBoNT/$B1_{MY}$, in a second common laboratory species. Because rat VAMP1 (vesicle associated membrane protein 1), the predominant isoform in motor neurons, has a mutation that renders skeletal

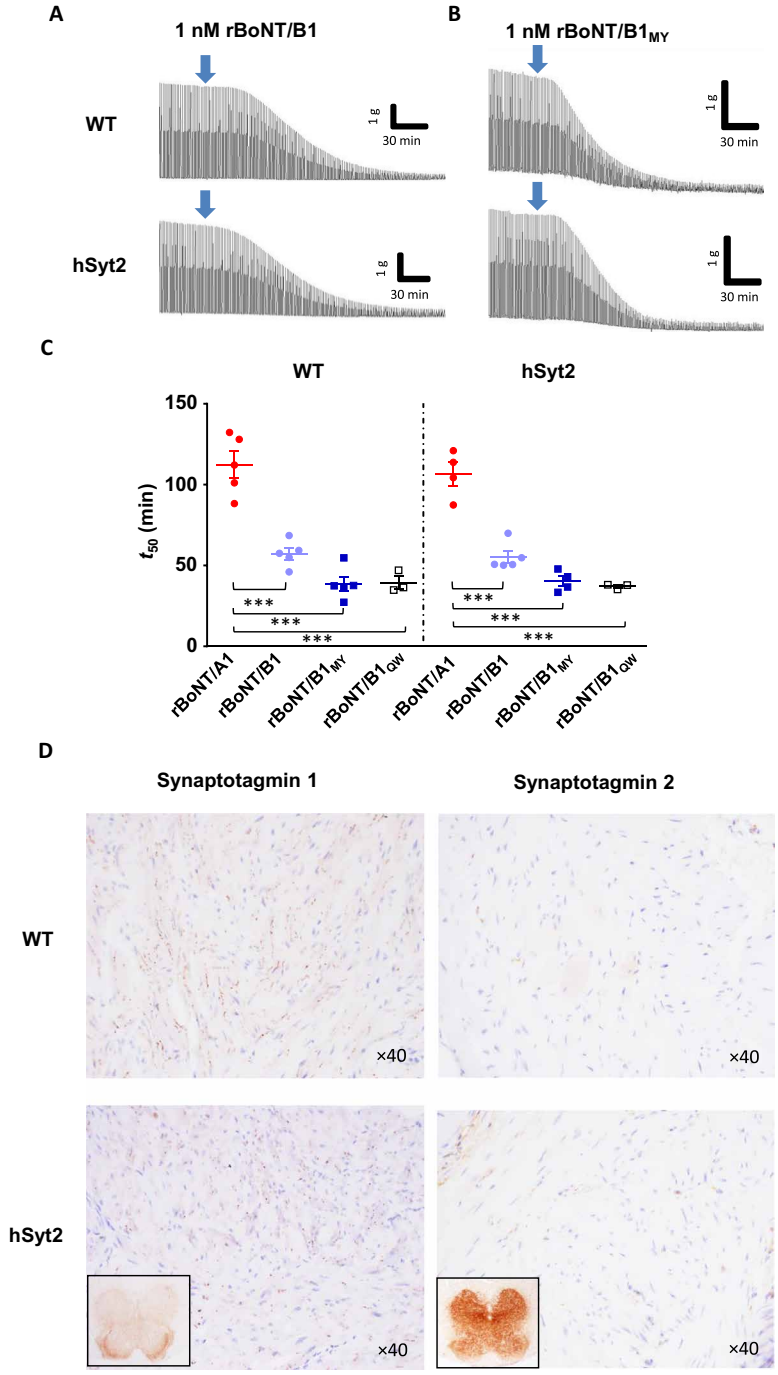

Fig. 4. Engineered rBoNT/B1, as well as rBoNT/B1, toxins induce rapid bladder detrusor muscle paralysis in hSyt2 mice. (**A** and **B**) Contractile force of bladder detrusor muscle strips plotted over time from WT or hSyt2 mice. Bladder detrusor muscles were electrically stimulated with 0.3-ms pulses at 10 Hz to determine the baseline contractile force. Following tissue stabilization, a toxin was added (blue arrows) to the bath at 1 nM final concentration. Both rBoNT/B1 (A) and rBoNT/B1$_{MY}$ (B) induced a comparable paralysis in bladder strip preparations from WT and hSyt2 mice. (**C**) All data were normalized to the contractile strength before toxin addition and fitted to a four-parameter equation to determine t_{50}. Between tissue types, there was no significant difference for any of the four toxins tested (unpaired *t* test). Datasets for all toxins per WT or hSyt2 mice were compared with ANOVA, followed by Tukey's test for multiple comparisons. ***$P < 0.0001$. All other comparisons were not significant. (**D**) IHC analysis of urothelium tissue shows low, consistent expression of Syt1 but fails to detect Syt2 in urothelium from WT and hSyt2 mice (inset: positive antibody control from spinal cord tissue).

muscles in rats insensitive to BoNT/B (*22*, *23*), we tested rBoNT/B1$_{MY}$ in a muscle force study in rabbits in which we evaluated potency, as well as the duration of action of the toxin. We compared the results to those obtained with rBoNT/A1 in the same model and at the same doses (Fig. 5B). Injection of rBoNT/B1$_{MY}$ induced a long-lasting, dose-dependent decrease in the muscle force of the treated hind limb. This decrease appeared similar in duration and strength to the decrease of muscle force induced by injections of rBoNT/A1 at

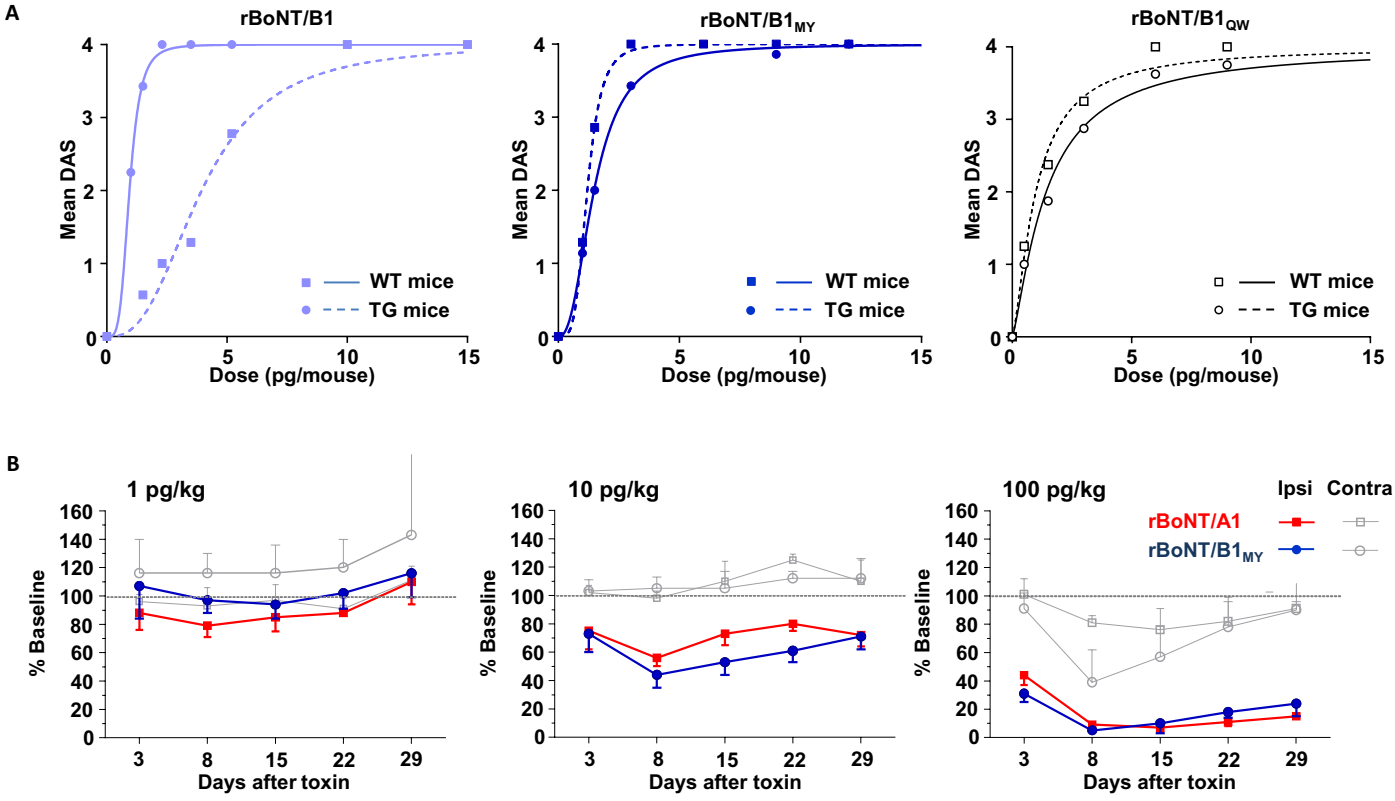

Fig. 5. Engineered rBoNT/B1 toxins have in vivo activity similar to rBoNT/A1. (**A**) rBoNT/B (left), rBoNT/B1$_{MY}$ (middle), and rBoNT/B1$_{QW}$ (right) were injected into the gastrocnemius-soleus muscle complex of the hind paw of WT or transgenic hSyt2 mice. DAS was scored daily during the first 4 days after injection, and the highest average DAS score per dose group during this period is plotted and fitted. ED_{50} values and lower and upper 95% confidence intervals derived from the fit are given in table S2. In the transgenic mice, rBoNT/B1 had dramatically reduced activity as compared to the WT animal. A high activity also in the transgenic animals was restored with both engineered toxins. (**B**) Muscle force generated in the hind leg of anesthetized New Zealand white rabbits after injection of rBoNT/A1 or rBoNT/B1$_{MY}$ into the gastrocnemius-soleus muscle complex of the hind paw. The muscle was stimulated at the tibial nerve with pulses of 40 V (50 μs at 0.5 Hz). The muscle force generated by the triceps surae group was recorded for at least 10 consecutive stimulations, and the maximum amplitude of the muscle force generated was calculated for each stimulation. Measurement was done for the side injected with the toxin [ipsilateral (Ipsi)], as well as the noninjected contralateral (Contra) side. Three doses were tested as indicated, and the muscle force was measured once weekly for 5 weeks.

all tested doses. Effects on the muscle force of the contralateral, noninjected, hind limb were seen for both toxins at 100 pg/kg but not at lower doses. This likely indicates systemic spread of the toxins at the 100 pg/kg dose, which therefore was the highest dose tested.

The key electrostatic interactions between BoNT/B1 and Syt are conserved in rBoNT/B1$_{MY}$

To obtain a mechanistic insight into the interaction of rBoNT/B1$_{MY}$ with hSyt2, we crystallized this toxin in complex with hSyt2 peptide (Fig. 6 and table S3). We also determined the x-ray crystal structure of Hc/B in complex with hSyt1 peptide to allow for a direct comparison. In all cases, the bound Syt peptides take on an α-helical structure and occupy the crevice at the tip of the binding domain, similar to what was previously reported for the binding of rat Syt2 to Hc/B (Fig. 6B) (*15*, *24*). The key electrostatic interactions between the toxin and all Syt peptide species are conserved between rBoNT/B and rBoNT/B1$_{MY}$; in particular, Syt E50$^{(hSyt1)}$/E54$^{(hSyt2)}$ forms salt bridges with K1113, S1116, and K1192 (figs. S3 and S4). The lysyl side chain of Syt K44$^{(hSyt1)}$/K48$^{(hSyt2)}$ is stabilized by E1203. The protein-peptide interface is mostly based on hydrophobic interactions, with two main pockets forming the receptor binding cleft. On one side, the conserved Syt F40$^{(hSyt1)}$/F44$^{(hSyt2)}$ occupies the subsite surrounded by Y1181, F1194, P1197, F1204, and position 1199. Replacement of the polar S1199 by an aromatic side chain (S1199Y) caused a slight outward shift of its carrying loop (1197-1201) and of the position of the N-terminal part of hSyt1 (Fig. 6C).

The second pocket is formed by residues V1118, Y1183, E1191, K1192, and F1994 and offers an important anchoring point for F47$^{(hSyt1)}$/L51$^{(hSyt2)}$. The E1191M mutation in rBoNT/B1$_{MY}$ provides greater hydrophobicity to this site (fig. S4). Replacement of this residue by methionine caused a significant repositioning of the charged side chain of E1191 from an outward-facing direction (in Hc/B) to a bulky side group (M1191) buried inside the pocket (Fig. 6C). The new interface in rBoNT/B1$_{MY}$ thus allows for stronger interaction with the hydrophobic side chains of L51$^{(hSyt1)}$/I55$^{(hSyt2)}$. This seems particularly important for hSyt2 recognition by rBoNT/B1$_{MY}$ where I55 is attracted deeper within the binding pocket, likely causing a slight transitional shift (1 Å) of the whole peptide compared to hSyt1 (Fig. 6D).

DISCUSSION

The present study investigates the effects of two modified rBoNT/B1 toxins, rBoNT/B1$_{MY}$ and rBoNT/B1$_{QW}$, both with higher affinity to hSyt1 and hSyt2 as compared to rBoNT/B1, in preclinical models.

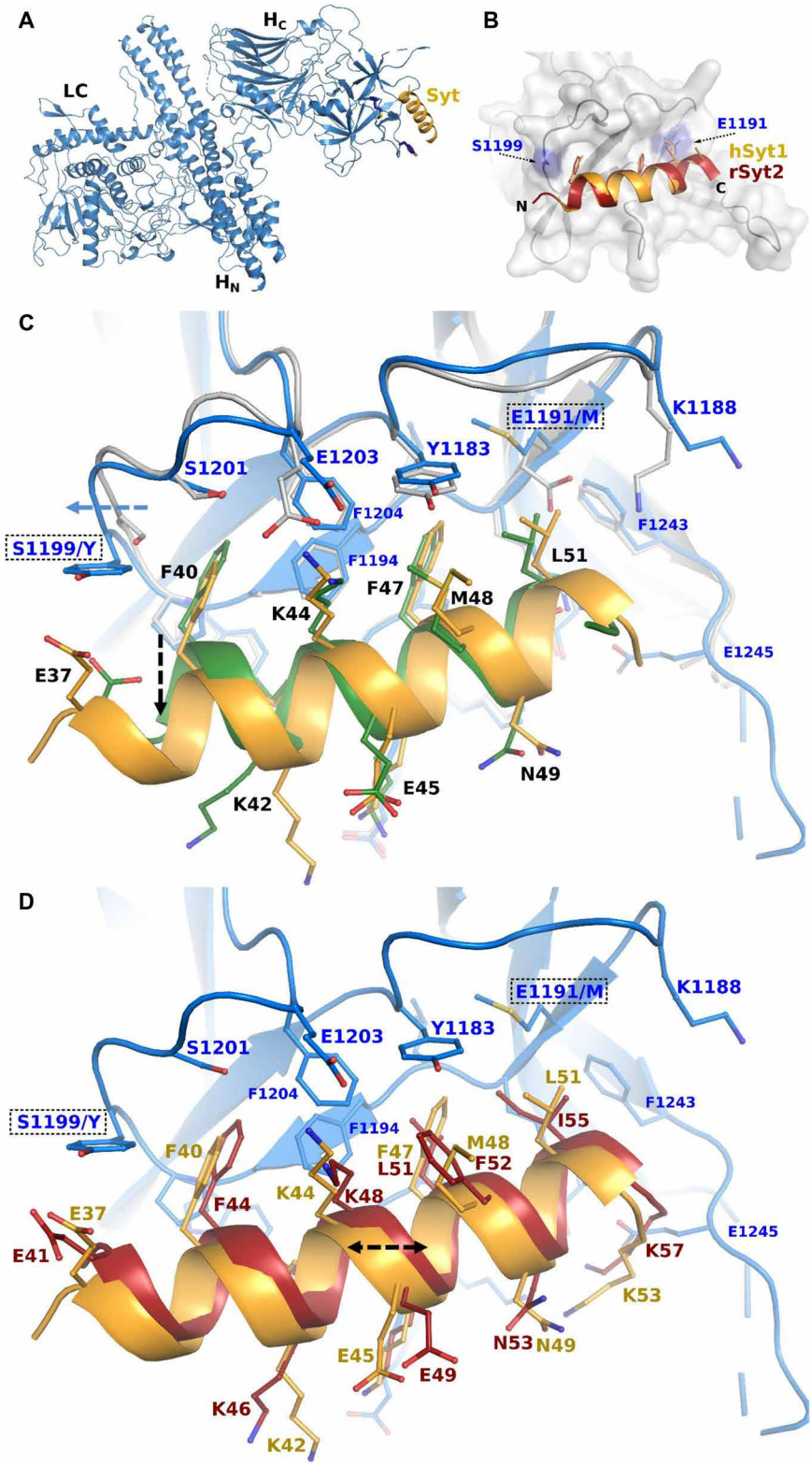

Fig. 6. Syt recognition by BoNT/B1 variants. (**A**) Crystal structure of rBoNT/B_{MY} (blue) in complex with hSyt1 (yellow). The three functional domains of BoNT/B1 are labeled, with the catalytic light chain (LC), the translocation domain (H_N), and the binding domain (H_C). (**B**) Superposition of the crystal structures of Hc/B (gray) with hSyt1 (yellow) and rSyt2 [red; Protein Data Bank (PDB) code: 2 nm1]. Structures were aligned using the binding domain only. Residues E1191 and S1199 are highlighted in blue; the N and C termini of Syt are indicated. (**C**) Superposition of the crystal structures of the Hc/B (gray)–hSyt1 (green) complex with rBoNT/B_{MY} (blue)–hSyt1 (yellow). Movement of loop 1197-1201 and the difference in the position of the peptides' N termini are indicated with blue and black arrows, respectively. (**D**) Superposition of the crystal structures of rBoNT/B_{MY} (blue) with hSyt1 (yellow) and hSyt2 (red). The shift between the two peptide positions is indicated with a black arrow.

Our main finding is that this improved affinity to the human receptors translates into increased activity in all models that express human Syt isoforms, including transgenic mice that express the hSyt2 toxin binding region. This finding shows that the neuronal binding step does limit the potency of BoNT/B in humans. This is also consistent with our recent finding that increasing the catalytic activity of rBoNT/B1 does not increase the activity in complex physiological systems and thus is not limiting the potency of BoNT/B (*25*).

We found a rather modest fourfold difference in the mouse DAS ED_{50} between rBoNT/A1 and rBoNT/B1 in the hSyt2 mice, as well as for rBoNT/B1 between the WT and hSyt2 mice. This contrasts with the roughly 40-fold conversion factor that is being used in clinical practice between BoNT/A1 and BoNT/B1 products for skeletal muscle indications (*3*). Although this may suggest that the low affinity of BoNT/B1 to hSyt2 is not the only reason for the low clinical efficacy of BoNT/B1, the hemidiaphragm data from the hSyt2 mice, the human-derived cell-based data, and the strong increase in Syt2 affinity do agree with the idea that the large difference between BoNT/A1 and BoNT/B1 in the clinic would mostly be due to the low affinity of BoNT/B1 to hSyt2. In this context, it is important to remember that the mouse DAS assay is performed on healthy mice. This model may be inadequate to predict clinical efficacy in spasticity at the quantitative precision required. There is clear evidence that spastic muscles show not only histopathological changes (*26*) but also changes in their transcriptional profile (*27*).

Another point of observation is that, in our previous study (*16*), we found that rBoNT/$B1_{MY}$ had ~11-fold higher activity than rBoNT/B1 using patch-clamp recording of miniature inhibitory postsynaptic currents in rat cortical neurons that express hSyt2 via lentivirus transduction. In the present study, we found an ~40-fold difference in activity between rBoNT/$B1_{MY}$ and rBoNT/B1 in hiPSCs using GABA release as a readout. This larger difference in the present study may simply be due to the different technologies used to measure activity. However, there are also other differences between the two studies. For example, the humanized model used in the earlier study expressed only hSyt2 but not Syt1 (*16*). In contrast, hSyt1 and hSyt2 are both present in iCell GABANeurons. Another difference between the studies is the presence of a C-terminal His-tag on the toxin used in our earlier study. While these tags are commonly used tools in the purification of recombinant proteins, they may alter the biological activity of purified proteins (*28*). We found that C-terminally histidine-tagged rBoNT/B1 and rBoNT/$B1_{MY}$ showed reduced potency than the untagged version in mouse hemidiaphragm preparations and in vivo in mice (fig. S5).

Our ex vivo data suggest that Syt2 is the dominant isoform mediating the paralyzing effects of BoNT/B in the hemidiaphragm. This is supported by studies showing expression of Syt2 at NMJs of striated muscle (*12*), including the hemidiaphragm (*29*). The presence of Syt1, also described in the latter tissue, is developmentally regulated with a strong down-regulation within the first 2 weeks after birth (*29*). Our studies, however, were performed on mice aged 5 to 6 weeks. In contrast, Syt1 seems to mediate the effect of BoNT/B in the urinary bladder tissue, and there is evidence that Syt1 is the predominant isoform in autonomic and sensory neurons (*30*). Our functional data are thus consistent with these earlier expression studies.

With regard to the ex vivo data, it is also interesting to note that the increase in affinity of the mutated toxins to hSyt2 as compared to the unmodified BoNT/B was reflected in the functional data in the hemidiaphragm data from the hSyt2 mice but that the increase in affinity of the mutated toxins to Syt1 as compared to the unmodified BoNT/B was not reflected on a statistical level by the functional data in the bladder strips preparation. This may be because the nerve endings in the bladder urothelium are embedded within the muscle structure, possibly leading to a dilution effect. This is likely to also account, at least in parts, for the higher toxin concentrations needed in this preparation as compared to the hemidiaphragm, where the NMJ of the phrenic nerve is easily accessible at the muscle surface.

By solving the crystal structures of H_C/B and rBoNT/$B1_{MY}$ bound to fragments of the human Syt receptors, we find that they bind to two hydrophobic pockets, which is consistent with previous structural studies with the homologous rat Syt2 receptor (*15*, *24*). Notably, the E1191M/S1199Y mutations do not perturb the network of electrostatic interactions seen between the native toxin and its receptor. Each mutation flanks the side of the binding crevice, providing additional hydrophobicity in key positions. For E1191M, the methionine improves hSyt2 binding by better accommodating L51 and I55 within the adjacent pocket and avoiding any conflict with the charged side chain of the glutamate. This in turn does not perturb the binding to hSyt1 that also presents hydrophobic residues in these positions (F47 and L51). On the other side of the crevice, the S1199Y mutation offers a bulky side group that widens the binding pocket and provides improved hydrophobic binding to $F40^{(hSyt1)}$/$F44^{(hSyt2)}$ of Syt. This position is highly conserved across Syt species; thus, it is unlikely that S1199Y plays a significant role in the observed variation in Syt specificity. Overall our crystal structures validate previous results in which rBoNT/$B1_{MY}$ showed improved affinity for hSyt2 and hSyt1 as compared to rBoNT/B1 (*16*). These detailed atomic structures of rBoNT/$B1_{MY}$ also offer a template to explore further mutations that could provide the toxin with enhanced receptor binding properties by, for example, targeting the plasticity of the loops surrounding the main site.

One unexpected consequence of generating hSyt2 mice was the observation of a partial infertility phenotype. While a previous study with a transgenic Syt2 mice also reported a decreased fertility (*31*), there was evidence that the specific mutation tested in this earlier study induced protein instability. Consequently, these transgenic mice not only showed fertility deficits but also had other gross phenotypic changes, such as small BW and ataxia, as well as reduced Syt2 protein expression (*31*). In contrast, besides a fertility phenotype, we did not observe other phenotypic changes with hSyt2 mice in the present study. Notably, the husbandry data can be explained by a simple dominant partial male infertility.

Our finding that rBoNT/$B1_{MY}$ and rBoNT/$B1_{QW}$ display high activity in all models that express human Syt isoforms suggests that these toxins could also have superior activity in the clinic, as compared to the currently available BoNT/B1 product. Our data allude to the possibility that the modified toxins may be as active as the BoNT/A1 products. Furthermore, the tolerability of these modified toxins in the preclinical studies was comparable to rBoNT/A1. Thus, modified rBoNT/B1 toxins with improved affinity to hSyt1 and hSyt2 may be viable alternatives to BoNT/A1 treatments, especially for patients who have developed neutralizing antibodies against BoNT/A1.

MATERIAL AND METHODS

Experimental design

The main objective of this study was to characterize the activity of two modified recombinant BoNT/B in several preclinical models,

including hiPSCs and a transgenic mouse with humanized Syt2 (hSyt2 mice), the major receptor for BoNT/B in skeletal muscle. The activity of the modified toxins was compared to unmodified BoNT/B1 and BoNT/A1. Last, we crystallized one of the recombinant modified BoNT/Bs to obtain mechanistic insight into how the modified BoNT/B interacts with its human receptor.

Cloning and expression of recombinant neurotoxins in *Escherichia coli* and their purification

The production of rBoNT/A1 (*32*) and rBoNT/B1 (*25*) has been described previously. In summary, constructs were cloned in the pET32a expression vector and mutations introduced by site-directed mutagenesis. Recombinant molecules were expressed in *E. coli* in selective media using 1 mM isopropyl-β-D-thiogalactopyranoside at 16°C for 20 hours. Cells were harvested and lysed, and the lysate was clarified before purification of target protein by fast protein liquid chromatography with BuHP Sepharose (GE Healthcare Life Sciences) and Q Sepharose High Performance (GE Healthcare Life Sciences). The partially purified molecule was then cleaved with Lys-C to yield the active di-chain, which was polished down a phenyl Sepharose High Performance (GE Healthcare Life Sciences) column. All recombinant toxins were purified and activated to more than 85%, as determined by densitometry, and molecule identity was confirmed by SDS–polyacrylamide gel electrophoresis (PAGE) and Western blot analysis (fig. S6, A and B).

The production of Hc/B was performed, as described previously (*15*). Briefly, the codon-optimized gene was cloned into the pET28a expression vector and expressed as above. Hc/B was purified by immobilized metal affinity chromatography with HisTrap HP (GE Healthcare Life Sciences), followed by gel filtration with Superdex 200 (GE Healthcare Life Sciences). The sample was kept in 20 mM Hepes (pH 7.5), 300 mM NaCl, 10% glycerol, and 0.5 mM TCEP [tris(2-carboxyethyl)phosphine].

Measurement of light-chain activity

The light-chain activities were assessed using the BoTest cell-free assay (BioSentinel, WI, USA), as previously described (*25*).

Glutathione *S*-transferase pull-down and biolayer interferometry assays

Glutathione S-transferase (GST) pull-down and biolayer interferometry assays were performed, as previously described (*16*).

X-ray crystallography

Samples for crystallization were prepared by preincubation of Hc/B (15 mg/ml) or rBoNT/$B1_{MY}$ (10 mg/ml) with 2 mM hSyt1 or hSyt2 peptides (GenScript, USA). Crystals were obtained from a sitting-drop vapor diffusion setup against Morpheus screen H5 (Molecular Dimensions, UK) for the Hc/B:hSyt1 complex; against 1.1 M sodium malonate dibasic monohydrate, Hepes (pH 7.0), and 0.5% (v/v) Jeffamine ED-2003 (JCSG screen, F10, Molecular Dimensions, UK) for the rBoNT/$B1_{MY}$:hSyt1 complex; and against 0.2 M magnesium chloride, tris (pH 7.0), and 10% (w/v) PEG 8000 (JCSG screen, B8, Molecular Dimensions, UK) for the rBoNT/$B1_{MY}$:hSyt2 complex. A drop of 200 nl of sample was mixed with an equal amount of reservoir and incubated at 16°C, and the crystal grew within 1 week. Crystals were transferred briefly into a cryoprotectant solution, consisting of their respective growth condition supplemented with 25% glycerol, before freezing in liquid nitrogen.

Diffraction data were collected at stations I02, I03, and I04–1 of the Diamond Light Source (Oxon, UK), equipped with a PILATUS-6M detector (Dectris, Switzerland). Complete datasets to 2.5 and 2.0 Å were collected from single crystals at 100 K for each complex. Raw data images were processed and scaled with XDS (*33*) or Mosflm (*34*), and Aimless (*35*) using the CCP4 suite 7.0 (*36*). The resolution cutoff chosen was based on the CC1/2 (*37*).

Molecular replacement was performed with the coordinates of BoNT/B (PDB code: 1EPW) (*38*) to determine initial phases for structure solution in Phaser (*39*). The working models were refined using Refmac5 (*40*) and manually adjusted with Coot (*41*). Validation was performed with MolProbity (*42*). Crystallographic data statistics are summarized in table S3. Figures were drawn with PyMOL (Schrödinger LLC, NY, USA).

Rat SCN culture and [^{3}H]-glycine release assay

All studies using rat SCNs were performed in the laboratories in the United Kingdom on material obtained from animals euthanized under Schedule 1 to the Animals (Scientific Procedures) Act 1986. Rat SCNs were prepared from E15 Sprague-Dawley rat embryos (Charles River, UK) and maintained in culture, as described previously (*25*).

Glycine release was assessed in SCNs at 20 to 23 days in vitro (DIV). Cells were treated with rBoNT/B1, rBoNT/$B1_{MY}$, or rBoNT/$B1_{QW}$ for 24 hours at 37°C. [^{3}H]-glycine release was determined, as described previously (*25*).

Release studies in iCell GABANeurons

iCell GABANeurons (Cellular Dynamics International, USA) were plated at a density of 60,000 cells per well in 96-well plates coated with poly-L-ornithine and laminin (Sigma-Aldrich, UK). iCell GABANeurons were maintained according to the manufacturer's instructions. iCell GABANeurons were fed every 3 to 4 days by replacement of half media.

GABA release was assessed in iCell GABANeurons at DIV 16 to 18. Cells were treated with neurotoxins for 24 hours at 37°C. Following removal of neurotoxin, cells were washed three times in Neurobasal medium containing 1% B27 and 0.5 mM GlutaMAX (assay medium). Cells were loaded with [^{3}H]-GABA (2 μCi/ml; PerkinElmer, UK) in assay medium for 120 min at 35°C. Following removal of [^{3}H]-GABA, cells were washed three times with assay medium. Basal and stimulated [^{3}H]-GABA release was established by incubation at 35°C for 5 min with assay medium (50 μl per well) containing low potassium (5.3 mM KCl) or high potassium (60 mM KCl), respectively. To determine retained [^{3}H]-GABA, cells were lysed by adding radioimmunoprecipitation assay buffer (50 μl per well; Sigma-Aldrich, UK). Superfusates and cell lysates were transferred into 96-well IsoPlates (PerkinElmer, UK), and OptiPhase Supermix scintillation fluid (200 μl per well) was added. Radioactivity was quantified using a MicroBeta2 plate reader (PerkinElmer, UK).

Generation of hSyt2 mice

The *Syt2* gene-targeting vector was constructed from genomic C57BL/6N mouse strain DNA (genOway, Lyon, France). Given that the intracellular and transmembrane regions of murine and hSyt2 are identical except for a single conservative amino acid substitution in the transmembrane region (see Fig. 2A), only the luminal domain of the protein was humanized. Humanization was achieved

by replacing the region coding for the luminal domain of the murine Syt2 protein (exon 4) with a complementary DNA (cDNA) encoding the human luminal domain, thus preserving the overall intron/exon structure of the murine gene. An FRT (flippase recognition target)–flanked neomycin cassette was inserted in intron 4. Access to the *Syt*2 knock-out was given by inserting *lox*P sites on each side of the exon 4 containing the ATG codon. Upon Cre-mediated excision, the humanized exon 4, containing the ATG codon and the neurotoxin interaction site, was deleted.

A linearized targeting vector was transfected into C57BL/6N embryonic stem (ES) cells (genOway, Lyon, France) per genOway's electroporation procedures. Recombined ES cell clones were microinjected into C57BL/6N blastocysts and gave rise to male chimeras with a significant ES cell contribution. Breeding was established with C57BL/6N mice expressing the Flp-recombinase to produce the *Syt*2 humanized heterozygous line devoid of the neomycin cassette. Heterozygous humanized animals were interbred to produce the *Syt*2 humanized homozygous line.

Handling of animals

Except for the muscle force studies on rabbits, all ex vivo and in vivo experiments were done within the Ipsen laboratory premises in France and were conducted in compliance with the relevant animal health regulation in place [Council Directive No. 2010/63/UE of 22 September 2010 on the protection of animals used for scientific purpose and Institutional Animal Care and Use Committee (IACUC) guidelines]. These studies were also approved by an internal ethics committee at Ipsen. Muscle force studies on rabbits were performed at Charles River Laboratories in Lyon, France. The study design was reviewed and approved by the ethical committee of the test facility of Charles River, was submitted to French authorities, and followed the IACUC guidelines.

For ex vivo or in vivo mouse studies, female C57BL/6N mice weighing 18 to 25 g were purchased from Charles River (Lyon, France) or Janvier (Le Genest-Saint-Isle, France) and allowed to acclimatize for at least 5 days before the experiments. Animals were housed with six mice per cage and acclimatized for 7 days before the beginning of the experiments. The mice had free access to water and were fed with pelleted complete diet ad libitum.

For rabbits muscle force test, male New Zealand white rabbits [Crl: KBL(NZW), 3.1 to 4 kg] were purchased from Charles River (Chatillon sur Chalaronne, France) and acclimatized for at least 7 days before the experiment. Animals were housed in individual cages, had free access to filtered (0.2 μm) mains drinking water, and were fed with pelleted complete rabbit diet, sterilized by irradiation, ad libitum. In addition, irradiated hay (Special Diet Services) was provided daily.

Phenotypic characterization of hSyt2 mice

Mice were euthanized by exsanguination under deep anesthesia. WT male and female mice were compared to hSyt2 mice. There were three mice per sex per group, and 51 tissue sections per animal were examined. Tissues were fixed in formalin or in Davidson's solution (eyes, lacrimal and Harderian glands, testes, and epididymides) for 24 hours and then embedded in paraffin. Tissue sections were hematoxylin and eosin–stained, and additional testicular sections were stained using periodic acid–Schiff for a better examination. Tissue sections were examined by a board-certified veterinary pathologist.

Immunohistochemistry

Tissue sections were deparaffinized and submitted to antigen retrieval treatments, as previously described (*43*). After two blocking steps with 3% H_2O_2 (Sigma-Aldrich) for 10 min, and 10% horse serum (Vector) for 30 min, slides were incubated for 60 min at room temperature with the primary antibody (table S4). A secondary biotinylated antibody (Vector Labs) was applied for 30 min, followed by detection (30 min) with an avidin/biotin system (VECTASTAIN ABC Elite, PK-7100, Vector). The signal was revealed with Dako Envision system using DAB substrate (3,3′-diaminobenzidine; K5007, Dako). Nuclei were stained with hematoxylin (K8018, Dako) for 3 min. Isotype controls immunoglobulins (Vector) were included in all experiments to attest of the specificity of the staining. Sections were dehydrated in the Leica AutoStainer XL and mounted with DPX Mountant (VWR International).

Mouse phrenic nerve hemidiaphragm and detrusor strip ex vivo organ bath assays

Preparation of mouse hemidiaphragm and mouse detrusor bladder strips and recordings from these tissues were done, as previously described (*19*, *25*).

Mouse DAS assay

The DAS assay (*20*, *44*) was used to test efficacy in mice in vivo, as described previously (*25*). Mice presenting an abnormal paw, or a control DAS score different from 0, were excluded. Mice were identified by a mark on the tail or via implanted ID microchips. In each study, experiments were performed on four to six mice per dose. Toxins were evaluated in hSyt2 mice and WT littermates in parallel. Mice were assigned to doses in a randomized manner. Two to three independent studies were performed for each toxin.

In parallel to the DAS measurements, mice were weighed daily. The variation of the BWs after treatments was calculated for each day from the baseline BW (before injections) for each mouse and then averaged in groups. The 0% BW dose was calculated for the day of the largest average percentage variation during the entire study by linear regression of the part of the curve covering 0% average percentage variation. The tolerability index of the toxins was subsequently calculated as the ratio of 0% BW and ED50.

Rabbit muscle force generation test

A method to measure the muscle force developed by the triceps surae group of the left and right hind limb was adapted to rabbits from a previously described rat model (*45*). Briefly, animals were anaesthetized with isoflurane (0.5 to 5%) in oxygen. The hair on each hind limb was clipped before the first experiment and as necessary during the study. Stimulation sites were identified by a spotted tattoo. Rabbits were placed onto a specially designed apparatus securing each hind limb such that only the tibiotarsal joint was mobile. An isometric force transducer (model K1000, HSE, Harvard Apparatus) was secured to the forefoot such that the tibiotarsal angle was at 90°. A pair of needle electrodes was then placed near the tibial nerve. The tibial nerve was electrically stimulated [square shocks, 40 V (50 μs at 0.5 Hz); Stimulator C type 224, HSE, Harvard Apparatus], and the muscle force was recorded using the force transducer connected to a computerized data acquisition system (Notocordhem software, NOTOCORD Systems S.A., Croissy-Sur-Seine, France). The signal was continuously sampled at 500 Hz and recorded from each animal twice for pretest measurement and then at days 3, 8, 15,

22, and 31 after injection. Animals were injected with the vehicle (Gelatin Phosphate Buffer) at a dose volume of 0.1 ml/kg in the left gastrocnemius muscle and BoNTs at a dose volume of 0.1 ml/kg in the right gastrocnemius muscle at day 1, under anesthesia. Absolute muscle force values were recorded for the vehicle- and toxin-injected hind limb. Data were normalized to the arithmetic mean of the pre-test measurements.

Expression analysis by Western blot in iCell GABANeurons and WT and hSyt2 mice

Proteins from the cortex, cerebellum, and hippocampus of six WT and eight hSyt2 mice were extracted from approximately 20 mg of each brain region in 500 µl of ice-cold T-PER (Tissue Protein Extraction Reagent; Thermo Fisher Scientific) supplemented with 10% of Complete Protease Inhibitor Cocktail (Roche) using Precellys (Ozyme).

iCell GABANeurons (Cellular Dynamics International) from three wells of six-well plates were harvested at 1, 7, 14, 21, and 28 days after plating in M-PER (Mammalian Protein Extraction Reagent; Thermo Fisher Scientific) supplemented with 10% of Halt Protease Inhibitor Cocktail (Thermo Fisher Scientific).

Proteins (20 µg) from each sample were resolved by SDS-PAGE (Invitrogen) and transferred onto nitrocellulose membranes. Membranes were blocked with 5% nonfat milk in 0.1% PBS-T (phosphate-buffered saline with Tween20) and probed with an anti-Syt1 antibody (1/1000; ab126253, Abcam) or anti-Syt2 antibody [sysy105123, SYnaptic SYstems (iCell GABANeurons) or sysy105223, SYnaptic SYstems (mice samples), both at 1/1000]. Immunoreactive bands were detected using horseradish peroxidase–conjugated secondary anti-mouse (1/1000; A4416, Sigma-Aldrich) or anti-rabbit (1/1000; A6154, Sigma-Aldrich) antibodies and SuperSignal (Thermo Fisher Scientific). Bands were visualized on a PXi imager (Ozyme), and intensities were normalized to glyceraldehyde-3-phosphate dehydrogenase (GAPDH) (1/1000; MAB374, Millipore) or SNAP-25 (1/1000; S9684, Sigma-Aldrich).

Expression analysis by RT-qPCR in iCell GABANeurons and WT and hSyt2 mice

Total RNA of iCell GABANeurons was isolated with the PicoPure RNA Isolation Kit (Applied Biosystems) at 1, 7, 14, 21, and 28 days after plating. Human adult total brain RNA (BioChain) was used as a positive control. cDNA was generated from 0.5 µg of RNA with a High-Capacity cDNA Reverse Transcription kit (Applied Biosystems). Reverse transcription quantitative polymerase chain reaction (RT-qPCR) was performed with the TaqMan Universal PCR Master Mix (Applied Biosystems) using the following TaqMan Human Gene Expression Assays: Syt1 (Hs00194572_m1), Syt2 (Hs00980604_m1), VAMP1 (Hs01042310_m1), VAMP2 (Hs00360269_m1), VAMP3 (Hs00922166_m1), SNAP25 (Hs00938962_m1), STX1A (Hs00270282_m1), STX1B (Hs01041315_m1), and GAPDH (Hs03929097_g1). Quantification was performed at a threshold detection line (C_t value). The C_t of each target gene was normalized to GAPDH housekeeping gene.

Statistical analysis

All data are expressed as individual data or as means ± SEM of n independent experiments. Concentration, dose, and time-response curves were fitted by a four-parameter logistic equation, and the pIC_{50}, t_{50}, or ED_{50} was calculated. The inclusion criterion was set at $R^2 > 0.900$. For statistical analysis, differences were determined by ANOVA with significance set at the level of $P < 0.05$. A Tukey's post hoc test for multiple comparisons was used to determine differences of the modified toxins against rBoNT/B1 and rBoNT/A1, as indicated. Differences between WT and hSyt2 mice were evaluated for each toxin in unpaired t tests. All data processing and statistical tests were done using GraphPad Prism version 7.04 (GraphPad Software Inc., La Jolla, CA, USA).

SUPPLEMENTARY MATERIAL

Supplementary material for this article is available at http://advances.sciencemag.org/cgi/content/full/5/1/eaau7196/DC1

Fig. S1. Longitudinal study of SNARE protein expression in iCell GABANeurons.
Fig. S2. Evaluation of Syt2 sequences with L54 in BoNT/B binding site.
Fig. S3. Molecular mechanisms of Syt recognition by BoNT/B1 variants.
Fig. S4. Electron density maps of the bound peptides and surface electrostatic potential of toxins.
Fig. S5. Effect of C-terminal histidine tag on rBoNT/B1 activity.
Fig. S6. Production of recombinant BoNTs.
Table S1. Dissociation constants (in micromolar) of rBoNT/B1 binding domains for human (*h*) and rodent (*r*) GST-tagged Syt1 and Syt2, measured by biolayer interferometry.
Table S2. Efficacy and safety of toxins in murine in vivo studies.
Table S3. X-ray crystallography: Data collection and refinement statistics.
Table S4. Antibodies used in immunohistochemistry studies.

REFERENCES AND NOTES

1. S. Chen, Clinical uses of botulinum neurotoxins: Current indications, limitations and future developments. *Toxins* **4**, 913–939 (2012).
2. D. Dressler, Clinical applications of botulinum toxin. *Curr. Opin. Microbiol.* **15**, 325–336 (2012).
3. J. J. Chen, K. Dashtipour, Abo-, inco-, ona-, and rima-botulinum toxins in clinical therapy: A primer. *Pharmacotherapy* **33**, 304–318 (2013).
4. O. Lange, H. Bigalke, R. Dengler, F. Wegner, M. deGroot, K. Wohlfarth, Neutralizing antibodies and secondary therapy failure after treatment with botulinum toxin type A: Much ado about nothing? *Clin. Neuropharmacol.* **32**, 213–218 (2009).
5. C. L. Comella, J. Jankovic, K. M. Shannon, J. Tsui, M. Swenson, S. Leurgans, W. Fan, Dystonia Study Group, Comparison of botulinum toxin serotypes A and B for the treatment of cervical dystonia. *Neurology* **65**, 1423–1429 (2005).
6. J. Ramirez-Castaneda, J. Jankovic, C. Comella, K. Dashtipour, H. H. Fernandez, Z. Mari, Diffusion, spread, and migration of botulinum toxin. *Mov. Disord.* **28**, 1775–1783 (2013).
7. M. A. Brodsky, D. M. Swope, D. Grimes, Diffusion of botulinum toxins. *Tremor Other Hyperkinet. Mov.* **2**, tre-02-85-417-1 (2012).
8. A. R. Bentivoglio, A. Del Grande, M. Petracca, T. Ialongo, L. Ricciardi, Clinical differences between botulinum neurotoxin type A and B. *Toxicon* **107**, 77–84 (2015).
9. R. R. Sloop, B. A. Cole, R. O. Escutin, Human response to botulinum toxin injection: Type B compared with type A. *Neurology* **49**, 189–194 (1997).
10. T. Nishiki, Y. Kamata, Y. Nemoto, A. Omori, T. Ito, M. Takahashi, S. Kozaki, Identification of protein receptor for *Clostridium botulinum* type B neurotoxin in rat brain synaptosomes. *J. Biol. Chem.* **269**, 10498–10503 (1994).
11. M. Dong, D. A. Richards, M. C. Goodnough, W. H. Tepp, E. A. Johnson, E. R. Chapman, Synaptotagmins I and II mediate entry of botulinum neurotoxin B into cells. *J. Cell Biol.* **162**, 1293–1303 (2003).
12. Z. P. Pang, E. Melicoff, D. Padgett, Y. Liu, A. F. Teich, B. F. Dickey, W. Lin, R. Adachi, T. C. Südhof, Synaptotagmin-2 is essential for survival and contributes to $Ca2^{+-}$ triggering of neurotransmitter release in central and neuromuscular synapses. *J. Neurosci.* **26**, 13493–13504 (2006).
13. L. Peng, R. P.-A. Berntsson, W. H. Tepp, R. M. Pitkin, E. A. Johnson, P. Stenmark, M. Dong, Botulinum neurotoxin D-C uses synaptotagmin I and II as receptors, and human synaptotagmin II is not an effective receptor for type B, D-C and G toxins. *J. Cell Sci.* **125**, 3233–3242 (2012).
14. J. Strotmeier, G. Willjes, T. Binz, A. Rummel, Human synaptotagmin-II is not a high affinity receptor for botulinum neurotoxin B and G: Increased therapeutic dosage and immunogenicity. *FEBS Lett.* **586**, 310–313 (2012).
15. R. P. A. Berntsson, L. Peng, M. Dong, P. Stenmark, Structure of dual receptor binding to botulinum neurotoxin B. *Nat. Commun.* **4**, 2058 (2013).
16. L. Tao, L. Peng, R. P.-A. Berntsson, S. M. Liu, S. Park, F. Yu, C. Boone, S. Palan, M. Beard, P.-E. Chabrier, P. Stenmark, J. Krupp, M. Dong, Engineered botulinum neurotoxin B with improved efficacy for targeting human receptors. *Nat. Commun.* **8**, 53 (2017).
17. R. C. M. Whitemarsh, M. J. Strathman, L. G. Chase, C. Stankewicz, W. H. Tepp, E. A. Johnson, S. Pellett, Novel application of human neurons derived from induced pluripotent stem

cells for highly sensitive botulinum neurotoxin detection. *Toxicol. Sci.* **126**, 426–435 (2012).
18. J. I. M. van Uhm, G. M. A. Beckers, W. J. van der Laarse, E. J. H. Meuleman, A. A. Geldof, J. A. Nieuwenhuijzen, Development of an in vitro model to measure bioactivity of botulinum neurotoxin A in rat bladder muscle strips. *BMC Urol.* **14**, 37 (2014).
19. J. Maignel-Ludop, M. Huchet, J. Krupp, Botulinum Neurotoxins Serotypes A and B induce paralysis of mouse striated and smooth muscles with different potencies. *Pharmacol. Res. Perspect.* **5**, e00289 (2017).
20. K. R. Aoki, A comparison of the safety margins of botulinum neurotoxin serotypes A, B, and F in mice. *Toxicon* **39**, 1815–1820 (2001).
21. Y. Torii, Y. Goto, S. Nakahira, S. Kozaki, R. Kaji, A. Ginnaga, Comparison of systemic toxicity between botulinum toxin subtypes A1 and A2 in mice and rats. *Basic Clin. Pharmacol. Toxicol.* **116**, 524–528 (2015).
22. G. G. Schiavo, F. Benfenati, B. Poulain, O. Rossetto, P. Polverino de Laureto, B. R. DasGupta, C. Montecucco, Tetanus and botulinum-B neurotoxins block neurotransmitter release by proteolytic cleavage of synaptobrevin. *Nature* **359**, 832–835 (1992).
23. L. Peng, M. Adler, A. Demogines, A. Borrell, H. Liu, L. Tao, W. H. Tepp, S. C. Zhang, E. A. Johnson, S. L. Sawyer, M. Dong, Widespread sequence variations in VAMP1 across vertebrates suggest a potential selective pressure from botulinum neurotoxins. *PLOS Pathog.* **10**, e1004177 (2014).
24. R. Jin, A. Rummel, T. Binz, A. T. Brunger, Botulinum neurotoxin B recognizes its protein receptor with high affinity and specificity. *Nature* **444**, 1092–1095 (2006).
25. M. Elliott, J. Maignel, S. M. Liu, C. Favre-Guilmard, I. Mir, P. Farrow, F. Hornby, S. Marlin, S. Palan, M. Beard, J. Krupp, Augmentation of VAMP-catalytic activity of botulinum neurotoxin serotype B does not result in increased potency in physiological systems. *PLOS ONE* **12**, e0185628 (2017).
26. R. L. Lieber, S. Steinman, I. A. Barash, H. Chambers, Structural and functional changes in spastic skeletal muscle. *Muscle Nerve* **29**, 615–627 (2004).
27. L. R. Smith, E. Pontén, Y. Hedström, S. R. Ward, H. G. Chambers, S. Subramaniam, R. L. Lieber, Novel transcriptional profile in wrist muscles from cerebral palsy patients. *BMC Med. Genomics* **2**, 44 (2009).
28. J. M. J. Dickson, W.-J. Lee, P. R. Shepherd, C. M. Buchanan, Enzyme activity effects of N-terminal his-tag attached to catalytic sub-unit of phosphoinositide-3-kinase. *Biosci. Rep.* **33**, e00079 (2013).
29. R. Tejero, M. Lopez-Manzaneda, S. Arumugam, L. Tabares, Synaptotagmin-2, and -1, linked to neurotransmission impairment and vulnerability in spinal muscular atrophy. *Hum. Mol. Genet.* **25**, 4703–4716 (2016).
30. J.-Y. Li, R. Jahn, A. Dahlström, Synaptotagmin I is present mainly in autonomic and sensory neurons of the rat peripheral nervous system. *Neuroscience* **63**, 837–850 (1994).
31. Z. P. Pang, J. Sun, J. Rizo, A. Maximov, T. C. Südhof, Genetic analysis of synaptotagmin 2 in spontaneous and Ca^{2+}-triggered neurotransmitter release. *EMBO J.* **25**, 2039–2050 (2006).
32. A. Hooker, S. Palan, M. Beard, Recombinant botulinum neurotoxin serotype A1 (SXN102342): Protein engineering and process development. *Toxicon* **123**, S40 (2016).
33. W. Kabsch, XDS. *Acta Crystallogr. D Biol. Crystallogr.* **66**, 125–132 (2010).
34. T. G. G. Battye, L. Kontogiannis, O. Johnson, H. R. Powell, A. G. W. Leslie, iMOSFLM: A new graphical interface for diffraction-image processing with MOSFLM. *Acta Crystallogr. D Biol. Crystallogr.* **67**, 271–281 (2011).
35. P. Evans, Scaling and assessment of data quality. *Acta Crystallogr. D Biol. Crystallogr.* **62**, 72–82 (2006).
36. Collaborative Computational Project Number 4, The CCP4 suite: Programs for protein crystallography. *Acta Crystallogr. D Biol. Crystallogr.* **50**, 760–763 (1994).
37. P. R. Evans, G. N. Murshudov, How good are my data and what is the resolution? *Acta Crystallogr. D Biol. Crystallogr.* **69**, 1204–1214 (2013).
38. S. Swaminathan, S. Eswaramoorthy, Structural analysis of the catalytic and binding sites of *Clostridium botulinum* neurotoxin B. *Nat. Struct. Biol.* **7**, 693–699 (2000).
39. A. J. McCoy, R. W. Grosse-Kunstleve, P. D. Adams, M. D. Winn, L. C. Storoni, R. J. Read, *Phaser* crystallographic software. *J. Appl. Cryst.* **40**, 658–674 (2007).
40. G. N. Murshudov, P. Skubák, A. A. Lebedev, N. S. Pannu, R. A. Steiner, R. A. Nicholls, M. D. Winn, F. Long, A. A. Vagin, *REFMAC*5 for the refinement of macromolecular crystal structures. *Acta Crystallogr. D Biol. Crystallogr.* **67**, 355–367 (2011).
41. P. Emsley, B. Lohkamp, W. G. Scott, K. Cowtan, Features and development of *Coot*. *Acta Crystallogr. D Biol. Crystallogr.* **66**, 486–501 (2010).
42. V. B. Chen, W. B. Arendall III, J. J. Headd, D. A. Keedy, R. M. Immormino, G. J. Kapral, L. W. Murray, J. S. Richardson, D. C. Richardson, *MolProbity*: All-atom structure validation for macromolecular crystallography. *Acta Crystallogr. D Biol. Crystallogr.* **66**, 12–21 (2010).
43. S. Lezmi, N. Rokh, G. Saint-Macary, M. Pino, V. Sallez, F. Thevenard, N. Roome, S. Rosolen, Chloroquine causes similar electroretinogram modifications, neuronal phospholipidosis and marked impairment of synaptic vesicle transport in albino and pigmented rats. *Toxicology* **308**, 50–59 (2013).
44. R. S. Broide, J. Rubino, G. S. Nicholson, M. C. Ardila, M. S. Brown, K. R. Aoki, J. Francis, The rat Digit Abduction Score (DAS) assay: A physiological model for assessing botulinum neurotoxin-induced skeletal muscle paralysis. *Toxicon* **71**, 18–24 (2013).
45. A. Pickett, R. O'Keeffe, A. Judge, S. Dodd, The in vivo rat muscle force model is a reliable and clinically relevant test of consistency among botulinum toxin preparations. *Toxicon* **52**, 455–464 (2008).

Acknowledgments: We thank J.-L. Blachon (Ipsen) for help with the statistical analysis and M. Norbert (genOway) for help with compiling the husbandry data for the hSyt2 mice. We thank the scientists at stations I02, I03, and I04-1 of Diamond Light Source, Didcot, Oxfordshire (UK) for support during data collection (allocations MX11265 and MX15806). **Funding:** M.D. acknowledges the grant support from the NIH (NS080833 and AI132387) and holds the Investigator in the Pathogenesis of Infectious Disease award from the Burroughs Wellcome Fund. P.S. acknowledges the support by the Swedish Research Council (2014–5667), the Wenner-Gren Foundation, and the Swedish Cancer Society. This study was supported by an industry-sponsored research grant from Ipsen to M.D. and a grant for a postdoctoral fellow to P.S. sponsored by Ipsen. **Author contributions:** M.E. performed all cell-based assays. C.F.-G. performed the mouse DAS studies. S.M.L. produced the toxins. J.M. performed all ex vivo organ bath studies. G.M. did the crystallization studies. C.N. and E.R. performed the RT-qPCR and Western blot studies. D.C. and S.L. performed the IHC studies. I.M. performed the light-chain activity tests. C.B. contributed to the crystal structure studies of the complex. S.Z. performed the GST and BLI (biolayer interferometry) studies. C.P. coordinated the rabbit muscle force studies. M.K., S.P., M.B., M.D., P.S., and J.K. conceived and oversaw the studies. J.K. wrote the paper with input from all authors. **Competing interests:** M.D. and P.S. are inventors on a patent related to this work filed by Harvard Medical School [no. WO2013180799 (A1), filed on 05 December 2013]. M.D. is also an inventor on an additional patent related to this work filed by Harvard Medical School [no. WO2016154534 (A1), filed on 29 September 2016]. M.E., C.F.-G., S.M.L., J.M., C.N., E.R., D.C., S.L., I.M., C.P., M.K., S.P., M.B., and J.K. are employees of Ipsen. The authors declare that they have no other competing interests. **Data and materials availability:** The crystal structures described in this paper are accessible under PDB codes 6G5F, 6G5G, and 6G5K. All data needed to evaluate the conclusions in the paper are present in the paper and/or the Supplementary Materials. Additional data related to this paper may be requested from the authors.

Submitted 9 July 2018
Accepted 6 December 2018
Published 16 January 2019
10.1126/sciadv.aau7196

Citation: M. Elliott, C. Favre-Guilmard, S. M. Liu, J. Maignel, G. Masuyer, M. Beard, C. Boone, D. Carré, M. Kalinichev, S. Lezmi, I. Mir, C. Nicoleau, S. Palan, C. Perier, E. Raban, S. Zhang, M. Dong, P. Stenmark, J. Krupp, Engineered botulinum neurotoxin B with improved binding to human receptors has enhanced efficacy in preclinical models. *Sci. Adv.* **5**, eaau7196 (2019).

Engineered botulinum neurotoxin B with improved binding to human receptors has enhanced efficacy in preclinical models

Mark Elliott, Christine Favre-Guilmard, Sai Man Liu, Jacquie Maignel, Geoffrey Masuyer, Matthew Beard, Christopher Boone, Denis Carré, Mikhail Kalinichev, Stephane Lezmi, Imran Mir, Camille Nicoleau, Shilpa Palan, Cindy Perier, Elsa Raban, Sicai Zhang, Min Dong, Pål Stenmark and Johannes Krupp

Sci Adv **5** (1), eaau7196.
DOI: 10.1126/sciadv.aau7196